Applied Physics Letters

Patterning and manipulating microparticles into a three-dimensional matrix using standing surface acoustic waves

Cite as: Appl. Phys. Lett. **112**, 213507 (2018); https://doi.org/10.1063/1.5024888
Submitted: 05 February 2018 . Accepted: 08 May 2018 . Published Online: 23 May 2018

T. D. Nguyen, V. T. Tran, Y. Q. Fu, and H. Du

Patterning and manipulating microparticles into a three-dimensional matrix using standing surface acoustic waves

T. D. Nguyen,[1] V. T. Tran,[2] Y. Q. Fu,[3] and H. Du[1,a)]
[1]*School of Mechanical and Aerospace Engineering, Nanyang Technological University, Singapore 639798*
[2]*Singapore Centre of 3D Printing, Nanyang Technological University, Singapore 639798*
[3]*Faculty of Engineering and Environment, Northumbria University, Newcastle upon Tyne NE1 8ST, United Kingdom*

(Received 5 February 2018; accepted 8 May 2018; published online 23 May 2018)

A method based on standing surface acoustic waves (SSAWs) is proposed to pattern and manipulate microparticles into a three-dimensional (3D) matrix inside a microchamber. An optical prism is used to observe the 3D alignment and patterning of the microparticles in the vertical and horizontal planes simultaneously. The acoustic radiation force effectively patterns the microparticles into lines of 3D space or crystal-lattice-like matrix patterns. A microparticle can be positioned precisely at a specified vertical location by balancing the forces of acoustic radiation, drag, buoyancy, and gravity acting on the microparticle. Experiments and finite-element numerical simulations both show that the acoustic radiation force increases gradually from the bottom of the chamber to the top, and microparticles can be moved up or down simply by adjusting the applied SSAW power. Our method has great potential for acoustofluidic applications, building the large-scale structures associated with biological objects and artificial neuron networks. *Published by AIP Publishing.*
https://doi.org/10.1063/1.5024888

Surface acoustic waves (SAWs)[1] are used to manipulate micro-sized objects precisely either in fluids within microchannels or in chambers on piezoelectric substrates.[2,3] SAW manipulation is compatible with living cells and other biological objects because its acoustic power intensity and frequency are similar to those used in ultrasonic imaging, which has been proven to be safe.[4] SAW-based devices can manipulate different types of microparticles of various shapes and mechanical, electrical, magnetic, and optical properties.[4] The SAW method is a contactless method that uses the generated acoustic pressure/force to manipulate the microparticles, thereby avoiding sample contamination and allowing the biological objects remain in their original environment. Because of its small scale, SAW manipulation involves relatively low power consumption and cost. Moreover, the radio frequency (RF) signal that powers up the interdigital transducers (IDTs) of a SAW-based device can be integrated easily with other programmable microfluidics and sensing techniques to open up a control strategy for lab-on-a-chip applications.[5] Because they operate at high acoustic frequencies, SAW-based devices can manipulate microparticles quickly and efficiently.[6] Cells and microparticles have been patterned in two dimensions by using two orthogonal pairs of IDTs.[3,7]

However, the use of SSAWs to manipulate microparticles in three dimensions has been rather limited to date. There was a report of trapping microparticles into nodes using "3D acoustic tweezers" which was created by locating two pairs of IDTs perpendicularly to each other.[8] These trapping nodes could be translated horizontally by changing the relative phases of the pairs of opposing IDTs. Thus, the microparticles trapped in the nodes were also transported accordingly. The trapped microparticles could also be levitated by increasing the input power applied to the IDTs. However, the vertical range of manipulation by this technique was quite limited (i.e., 100 μm). With a taller chamber, the reflection of acoustic waves from the top wall changed the acoustic field therein. Therefore, the vertical distribution of microparticles in the chamber differed from that predicted based on the above "3D acoustic tweezers" model.

To date, no studies have explored using SSAWs to manipulate and distribute microparticles in chambers of millimeter-scale height. In this letter, we investigate the three-dimensional (3D) motions of polystyrene microparticles inside a 1-mm-tall chamber and the influence of the RF power by selecting a suitable microchamber geometry and acoustic frequencies. We also use a simplified numerical model to investigate the SAW acoustic field and the motions of microparticles under the acoustic radiation force. Our proposed manipulation could be used extensively to build the large-scale structures associated with biological objects and artificial neuron networks of neuron cells without harming them. It could also have a wide range of applications in acoustofluidics and lab-on-a-chip technology.

Fig. 1(a) shows a schematic of the SAW-based microchannel device used in this study, and Fig. 1(b) shows an optical image of the assembled SAW system. The piezoelectric substrate is 128° Y-cut lithium niobate ($LiNbO_3$). The IDTs were patterned using standard photolithography followed by a lift-off process to obtain metal electrodes (Cr/Au, 10 nm/50 nm) on the $LiNbO_3$ wafer. The IDTs have 60 pairs of fingers with both a width and space gap of 75 μm, corresponding to a SAW wavelength of 300 μm and an aperture of 1 cm. To make the lines of trapped microparticles parallel to the IDT fingers, we aligned a cubic polydimethylsiloxane (PDMS) chamber (Sylgard 184 Silicone Elastomer; Dow Corning, USA) with the IDT patterns and bonded it on top of

a)Author to whom correspondence should be addressed: MHDU@ntu.edu.sg

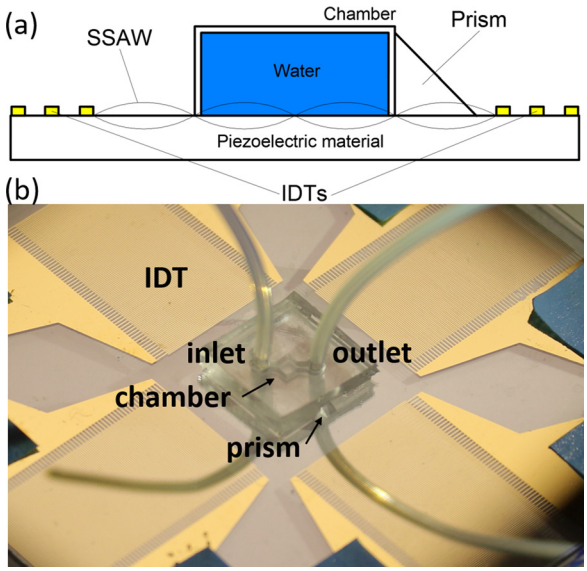

FIG. 1. (a) Schematic of the surface acoustic wave (SAW)-based device. (b) Optical image of the device after fabrication, showing interdigital transducers (IDTs), polydimethylsiloxane (PDMS) chamber, prism, inlet, and outlet.

the piezoelectric substrate after plasma treatment (Fig. 1(b)). The chamber is 1.5 mm wide (covering five SAW wavelengths) and 1 mm tall and was prepared using soft casting with a computer numerical controlled (CNC)-made mold. We used a signal generator (MHS-5200P; Ming Wo Electronics, China) to create an RF sine-wave signal that was amplified by an RF amplifier (the amplifier characteristics are provided in Fig. S1 in the supplementary material) before being applied to the IDTs to generate the SAWs. We measured the resonant frequency using an impedance analyzer (4294A precision impedance analyzer; Agilent, USA). We performed frequency-sweep measurements to scan a wide frequency range, and resonance occurred at the highest impedance. The results of these measurements are presented in Figs. S2 and S3 in the supplementary material; the resonant frequencies for the IDT pairs along two orthogonal directions were measured to be 13.30 MHz and 12.35 MHz. We injected microparticles of two different sizes (polybead microspheres; average diameters: 10 μm and 20 μm; Polysciences, USA) dispersed uniformly in water into the chamber using a syringe pump (LSP02-1B dual-channel syringe pump; LongerPump, China). To record the microparticle trajectories, we connected a charge-coupled device (CCD) camera (Andor iXonEM+; Oxford Instruments, UK) to a microscope (Eclipse Ti-U inverted microscope; Nikon, Japan). A challenge in monitoring the vertical microparticle behavior was that the microscope only allowed observation in the horizontal plane with a short focal distance. Therefore, we used a right-angle prism (N-BK7 right-angle prism; length of 1 mm, Edmund Optics, USA) to reflect the light through an angle of 90° to the lens of the microscope [Fig. 3(a)]. We also placed a horizontal light source on the plane of the microscope to allow observation over the x-y plane.

Before conducting the experimental work, we performed numerical modeling using the finite-element method integrated in commercial software (COMSOL) to understand the underlying physics of the acoustic radiation force exerted on the microparticles in the microchannel. Because the SSAW is uniform along the propagation direction of the channel, we simplified the chamber in the simulations to a 2D rectangular domain when viewed from the side [Fig. 1(a)],[9] with dimensions of 1000 μm × 600 μm (height × width). In the numerical studies, we solved the Helmholtz equation for a damped wave with specific liquid and boundary conditions within the domain to obtain the first-order acoustic pressure and velocity.[10] Following Gor'kov,[11] we calculated the acoustic radiation force arising from the acoustic pressure exerted on the incompressible spherical microparticles whose diameters are less than the wavelength of the acoustic device. This acoustic radiation force pushes the microparticles into the trapping nodes. More details about the establishment of the Helmholtz equation and acoustic radiation force are presented in the section on the governing equations in the supplementary material. We applied the following boundary conditions. The bottom edge of the simulation domain was given an actuation boundary condition to simulate the substrate vibrating with a frequency of 13.32 MHz, corresponding to a wavelength of 300 μm. Because the PDMS chamber had significant radiative energy losses, therefore, the other edges were given the impedance boundary condition to simulate the PDMS walls. Citsabehsan *et al.* described the boundary conditions in full.[12] The parameters used in the numerical study are given in Table S1 in the supplementary material. In the COMSOL Multiphysics software, we used a module called "Pressure Acoustic" to solve for the acoustic pressure field and first-order velocity in the frequency domain, and then, we used the "Particle Tracing" module to track the microparticles. We conducted a mesh independence test to ensure that the solution was independent of the mesh resolution. We used triangular meshes with a maximum element length of 1 μm to ensure the accuracy of the numerical study. The numerical results shown in Fig. 2(a) indicate that the interaction of the SSAW with the liquid in the chamber results in an acoustic pressure field that is distributed periodically in both the horizontal and vertical directions when viewed from the side. Because of the pressure field, the generated acoustic radiation force pushes the microparticles toward the pressure nodes. Fig. 2(b) shows the potential field of the acoustic radiation force, namely, $U = -\nabla F$.[11] In this potential field, the acoustic radiation force is directed from higher potential (red) to lower potential (blue). Fig. 2(c) shows the directions of the acoustic radiation forces exerted on a single microparticle in a balanced state in the acoustic potential field. Finally, Fig. 2(d) shows the final positions of the 10-μm microparticles after applying SAW power for 10 s.

In the experimental work, because the PDMS chamber is transparent, the light from the light source can travel through the chamber to the prism, where it is bent by 90° toward the microscope lens [Fig. 3(a)]. Figs. 3(b)–3(d) show different views (along the x, y, and z directions, respectively) of the 10-μm microparticles in the chamber after the RF signal was switched on. On combining the three views, the results showed clearly that the microparticles aggregated into 3D lines distributed equally from top to bottom and also in the x direction [Fig. 3(a)]. In the vertical direction, there were ~14 parallel lines of microparticles with a distance of ~60 μm between two adjacent lines. This

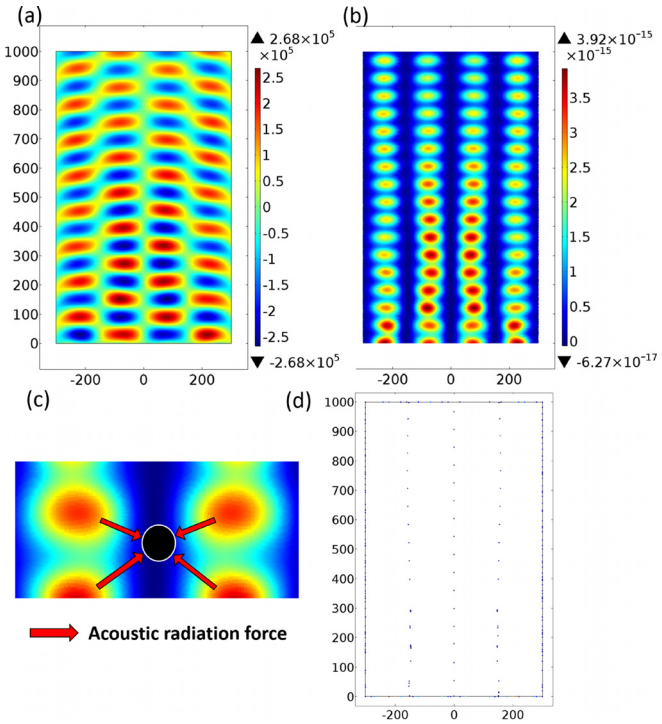

FIG. 2. (a) Acoustic pressure; colors show magnitude from −0.268 MPa (blue) to 0.268 MPa (red). (b) Radiation force potential; colors show magnitude from −6.27 × 10–17 J (blue) to 3.92 × 10–15 J (red). (c) Directions of acoustic radiation forces. (d) Numerical results for motion of 10-μm microparticles after 10 s; there are 1421 microparticles, and the initial (0 s) distance between two adjacent microparticles was 20 μm.

distance can be calculated approximately using $\lambda = v/f$, where λ is the wavelength in the vertical direction, v is the speed of sound in water (∼1502 m/s), and f is the operating frequency (13.32 MHz). On the horizontal plane, the distance between two adjacent lines was 150 μm, which is half the wavelength. Therefore, there were ∼10 lines over the chamber length of 1500 μm. With an input power of 3500 mW, the microparticles were aligned completely with the nodes after 4.5 s. Clearly, the experimental and numerical results agree well regarding the number of layers and the distance between adjacent lines. Regarding the microparticle trajectories, the microparticles were moved into vertical lines and then separated into layers, which matches well with the observation in Fig. 3(c). The numerical results for the microparticle trajectories are shown in Fig. S4 in the supplementary material. Moreover, we obtained 3D images of these 3D lines by capturing images sequentially at different focal depths along the y axis. The detailed 3D image is shown in Fig. S5 in the supplementary material. Based on the experimental observations, the acoustic radiation force is the most significant force acting on the microparticles after those of gravity and buoyancy. Fig. 4 illustrates all the forces acting on a microparticle in the balanced state in the x and z directions. The total force is zero in the x direction because the two equal and opposite acoustic radiation forces cancel each other. In the z direction, the microparticle is subjected to two upward forces (i.e., the upward acoustic radiation force and buoyancy) and two downward forces (i.e., the downward acoustic radiation force and the gravitational force). The sum of the gravitational and buoyancy forces is a net downward

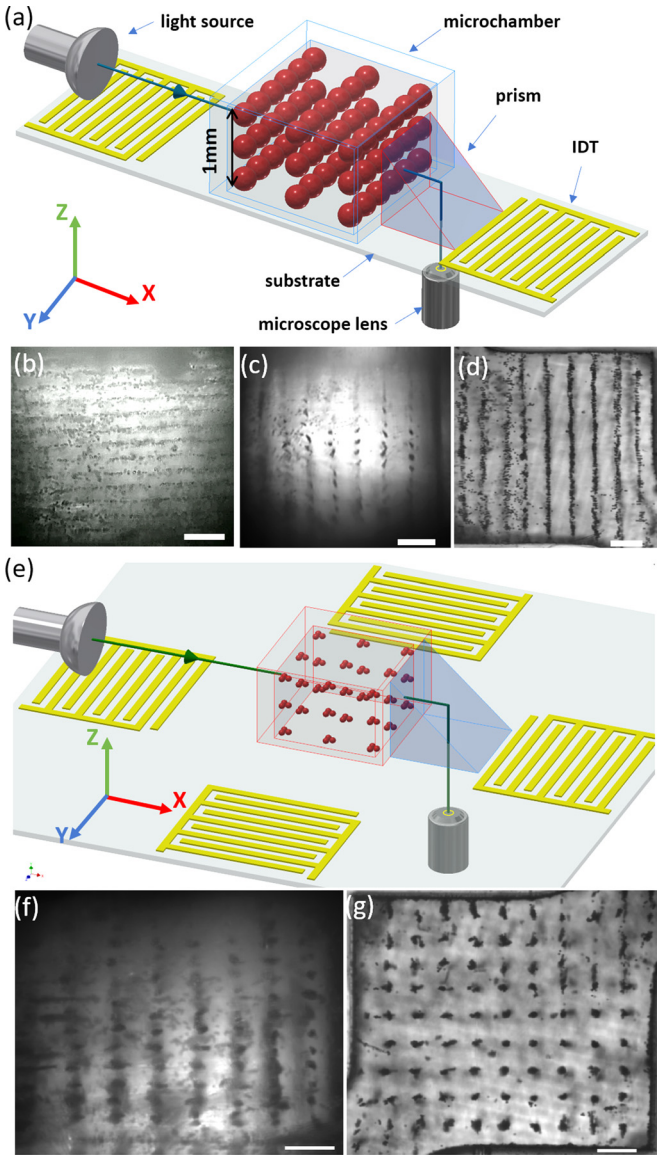

FIG. 3. (a) Schematic of the experimental setup for observing 3D lines of 10-μm-microparticles from the side using the prism. (b)–(d) Microscopy images of 3D lines of 10-μm microparticles after introducing an SSAW with an input power of 3500 mW viewed from x, y, and z directions, respectively (scale bar: 200 μm). (e) Visualization of 3D patterning by powering on two pairs of IDTs. (f) and (g) Microscopy images of 3D patterning viewed from the x and y directions, respectively (scale bar: 200 μm).

force $F_D = Vg(\rho_P - \rho)$, where V is the particle volume, g is the gravitational acceleration, $\rho_P = 1.12$ g/ml is the particle density, and $\rho = 1$ g/ml is the density of the medium. This net force depends strongly on the particle volume. Furthermore, because the acoustic radiation force is stronger nearer the bottom of the chamber [Fig. 2(b)], the sum of the upward and downward acoustic radiation forces is net upward force F_U that depends on both the vertical position of the microparticles (i.e., the higher the position, the weaker the force) and the input power (i.e., the higher the input power, the higher the radiation force potential). Consequently, when the downward force F_D and the upward force F_U are balanced (i.e., $F_D = F_U$), 3D lines of microparticles can form and be distributed both vertically and horizontally, as shown in Fig. 3(a).

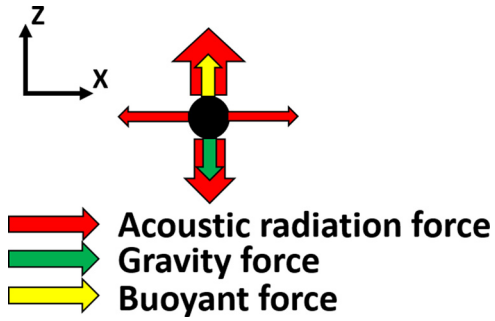

FIG. 4. Force analysis for a single microparticle in the z and x directions.

Similar to reports in the literature,[7,8,13,14] when the two orthogonal pairs of IDTs are supplied with the signal simultaneously, the microparticles aggregate at the nodes to form 2D horizontal patterns. Because the intersection of two orthogonal pressure lines forms a pressure node, the microparticles form 2D matrix patterns under the bi-directional acoustic radiation force. The prism used in this work afforded us side views of the distributions of microparticles in the chamber. Figs. 3(f) and 3(g) show side and vertical views, respectively, of the chamber when the two IDT pairs were supplied with RF power. Consequently, the microparticles not only aggregated to the nodes of 2D patterns but also formed 3D structures that resembled crystal lattices, as shown in Fig. 3(e). The uniformity of such 3D structures is affected by (i) microparticle aggregation at the nodes (which could lead to an increase in weight and fall to the bottom of aggregated particles), (ii) any instability in the RF signal, and (iii) any distortion of the chamber shape. Using smaller microparticles (i.e.; 1 μm) reduced the acoustic radiation force significantly, whereupon the 3D patterns disappeared completely. Instead, significant acoustic streaming was observed that caused closed-loop streaming inside the chamber.

The acoustic radiation force is affected significantly by the input power generated from the IDTs. In fact, the larger microparticles (e.g., 20 μm or sometimes 10 μm) tended to aggregate into even-larger composite particles (thereby increasing the effective particle weight) that would eventually fall to the bottom of the device. Thus, it was difficult to observe the 3D patterning of the larger microparticles when the input power was changed. Instead, by tracking the motion of a specific group of microparticles in the side view of the x direction while decreasing the input power, the microparticle motion clearly depended on the input power. Fig. 5(a) shows that a group of 10-μm microparticles moved to a lower vertical position in the layer order when the RF input power was decreased from 954 mW to 450 mW; the group fell onto the substrate if the input power was below 450 mW. Layer 14 is clearly the highest layer in this case, and layer zero is the substrate. Meanwhile, Fig. 5(b) shows that a single 10-μm microparticle moved upward from the bottom (substrate) when a constant RF input power of 4380 mW was applied. We observed that after the RF input power was turned on, the single microparticle moved gradually upward, reaching an equilibrium height of 524 μm after 31.4 s. The experimental results showed that the highest position that a microparticle can reach depends strongly on the input power. This demonstrates the ability to use an SSAW to control the 3D vertical positions of microparticles in a wide range (up to 1 mm in height). Therefore, we have established an effective way to manipulate relatively large microparticles in millimeter-size spaces. Precise control of microparticles on the horizontal (x-y) plane is easily realized and has been reported variously.[8,14] Herein, we have demonstrated that the vertical positions of microparticles can be controlled precisely and manipulated by adjusting the input power.

Our method differs from those published previously because (i) we can accommodate greater heights (i.e., up to ~1 mm) and (ii) our principle is to manipulate microparticles to the desired layer height by adjusting the input power. For example, a single 20-μm microparticle can be controlled to a different height (layer) by switching the input power on/off (Fig. 6, Multimedia view). The RF signal was turned off (SAW OFF) to let the microparticle fall and then switched on with an input power of 585 mW to hold the microparticle at the nearest layer. Finally, the microparticle was moved upward to the highest layer by switching on a higher input power of 1378 mW. Certainly, if the SSAW device were to be used for living cells, the input RF power would have to be controlled precisely

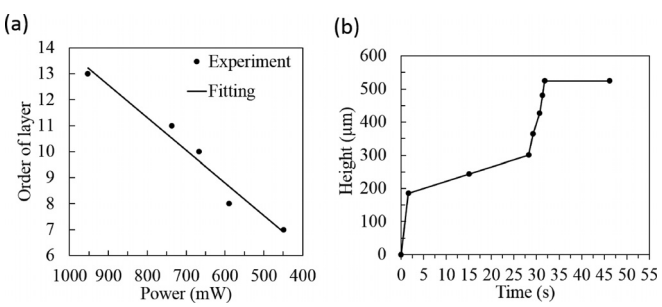

FIG. 5. (a) Changes of layer order of 10-μm microparticles when input power was decreased (side view of the X axis). (b) Levitation height of 10-μm microparticles from the bottom layer with time for an input power of 4380 mW.

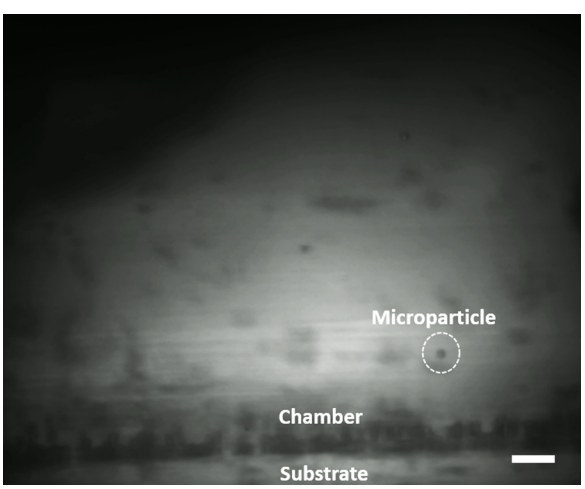

FIG. 6. A video shown a single 20-μm microparticle trapped at a 3D node by switching on the input power. Multimedia view: https://doi.org/10.1063/1.5024888.1

because otherwise it would pose a risk to the viability of the living cells because of heating effects.[15]

Therefore, more work is required to investigate how the input power affects the viability of cells during the 3D manipulation process.

In summary, we have demonstrated in this article that 3D patterning of lines and a lattice matrix of microparticles can be achieved in microfluidic devices using SSAWs. The mechanism for forming 3D lines of microparticles was investigated both experimentally and numerically, and both sets of results agreed well. We investigated thoroughly how the input power influenced the formation of 3D lines or layers, finding that the higher the input power, the stronger the acoustic radiation force. The acoustic radiation force increased gradually from the bottom of the chamber to the top, and the microparticles could be levitated to higher positions by simply increasing the power. A microparticle could be positioned precisely at a specified location if the total force (comprising those of the acoustic radiation, buoyancy, and gravity) acting on the microparticle was zero. Thus, a single microparticle could be positioned as desired by either (i) alternately switching on and off or (ii) adjusting the RF power.

See supplementary material for more details about establishing the Helmholtz equation, measuring the resonant frequency, the amplifier characteristics, the parameters used in the numerical model, the microparticle trajectories from the numerical study, and the 3D image of the 3D lines.

This research was supported by (i) Nanyang Technological University and the Ministry of Education of Singapore through a Ph.D. scholarship and (ii) UK Engineering and Physical Sciences Research Council (EPSRC EP/P018998/1).

[1]Y. Q. Fu, J. K. Luo, N. T. Nguyen, A. J. Walton, A. J. Flewitt, X. T. Zu, Y. Li, G. McHale, A. Matthews, E. Iborra *et al.*, Prog. Mater. Sci. **89**, 31 (2017).
[2]J. Friend and L. Y. Yeo, Rev. Mod. Phys. **83**(2), 647 (2011).
[3]L. Y. Yeo and J. R. Friend, Ann. Rev. Fluid Mech. **46**(1), 379 (2014).
[4]X. Ding, P. Li, S.-C. S. Lin, Z. S. Stratton, N. Nama, F. Guo, D. Slotcavage, X. Mao, J. Shi, F. Costanzo *et al.*, Lab Chip **13**(18), 3626 (2013).
[5]L. Meng, F. Cai, J. Chen, L. Niu, Y. Li, J. Wu, and H. Zheng, Appl. Phys. Lett. **100**(17), 173701 (2012).
[6]T. M. Squires and S. R. Quake, Rev. Mod. Phys. **77**(3), 977 (2005).
[7]J. Shi, D. Ahmed, X. Mao, S.-C. S. Lin, A. Lawit, and T. J. Huang, Lab Chip **9**(20), 2890 (2009).
[8]F. Guo, Z. Mao, Y. Chen, Z. Xie, J. P. Lata, P. Li, L. Ren, J. Liu, J. Yang, M. Dao *et al.*, Proc. Natl. Acad. Sci. **113**(6), 1522 (2016).
[9]Z. Mao, Y. Xie, F. Guo, L. Ren, P.-H. Huang, Y. Chen, J. Rufo, F. Costanzo, and T. J. Huang, Lab Chip **16**(3), 515 (2016).
[10]H. Bruus, Lab Chip **12**(1), 20 (2012).
[11]L. P. Gor'kov, Sov. Phys. Doklady **6**, 773 (1962).
[12]C. Devendran, T. Albrecht, J. Brenker, T. Alan, and A. Neild, Lab Chip **16**(19), 3756 (2016).
[13]S. M. Naseer, A. Manbachi, M. Samandari, P. Walch, Y. Gao, Y. S. Zhang, F. Davoudi, W. Wang, K. Abrinia, J. M. Cooper *et al.*, Biofabrication **9**(1), 015020 (2017).
[14]X. Ding, S.-C. S. Lin, B. Kiraly, H. Yue, S. Li, I.-K. Chiang, J. Shi, S. J. Benkovic, and T. J. Huang, Proc. Natl. Acad. Sci. **109**(28), 11105 (2012).
[15]H. Li, J. Friend, L. Yeo, A. Dasvarma, and K. Traianedes, Biomicrofluidics **3**(3), 034102 (2009).